The role of medium range order on phase transitions in chain silicates upon compression

2004 J. Phys.: Condens. Matter 16 S1255

(http://iopscience.iop.org/0953-8984/16/14/037)

INSTITUTE OF PHYSICS PUBLISHING JOURNAL OF PHYSICS: CONDENSED MATTER

J. Phys.: Condens. Matter **16** (2004) S1255–S1261 PII: S0953-8984(04)75043-2

The role of medium range order on phase transitions in chain silicates upon compression

G Serghiou[1], A Chopelas[2] and R Boehler[3]

[1] School of Engineering and Electronics and Centre for Materials Science, University of Edinburgh, EH9 3JL, UK
[2] Department of Physics, University of Washington, Seattle, WA 98195-1560, USA
[3] Max-Planck Institute for Chemistry, Postfach 3060, Mainz 55020, Germany

Received 22 January 2004
Published 26 March 2004
Online at stacks.iop.org/JPhysCM/16/S1255
DOI: 10.1088/0953-8984/16/14/037

Abstract

Raman spectroscopic measurements of the tetrahedrally coordinated crystal $MnSiO_3$ (rhodonite) in an argon pressure medium show that it becomes amorphous above 33 GPa. This observation consolidates our findings and explanation for the global structural trends exhibited by the extended chain silicate family $AA'BO_3$ (A, A′: Mg, Ca, Mn, Fe; B: Si) upon compression. In particular, crystals of this family are made of two types of building blocks coined P and C. Those crystals comprised solely of P blocks transform to dense higher coordinated crystalline phases; those comprised of P and C blocks, such as $MnSiO_3$ rhodonite, become amorphous; whereas those comprised solely of C blocks show both crystalline and amorphous regions upon compression. The reason that this medium range order length scale (building block scale) classification is correlated with the type of transitions taking place upon compression is due to the instability of C blocks and C–P interfaces with respect to P blocks and P–P interfaces at high pressures.

1. Introduction

Chain silicates of the family $AA'BO_3$ (A, A′: Mg, Ca, Mn, Fe; B: Si) have been the focus of intense interest in a variety of fields. From the materials science point of view, non-crystalline $CaSiO_3$ was one of the first materials shown to exhibit medium range structural order similar to that of its crystalline analogue [1]. From the planetary science point of view, $MgSiO_3$ pyroxene is a principal component of the Earth's upper mantle [2] and also one which transforms, at greater depths (>670 km) at temperatures exceeding 1800 K, to the most abundant solid of our planet, namely, octahedrally coordinated (SiO_6) $MgSiO_3$ perovskite [3]. From the crystal chemical point of view, chain silicates exhibit a rich, yet elegantly simple, structural taxonomy. They consist of chains of corner connected SiO_4 tetrahedra which run parallel to the crystallographic *c*-axis. These chains are separated from each other by layers

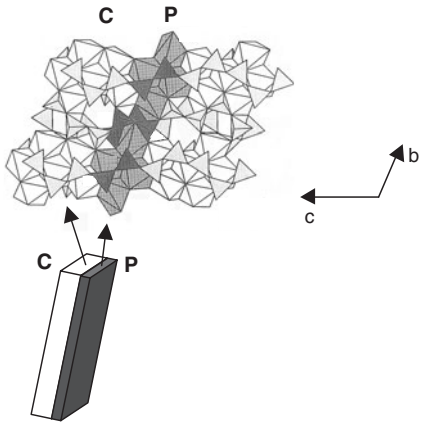

Figure 1. $MnSiO_3$ pyroxmangite projected onto the *b*–*c* plane. The larger polyhedra are Mn–O octahedra and the smaller polyhedra depicted by triangles are SiO_4 tetrahedra. The tetrahedra are corner connected to each other by sharing an oxygen, and form chains running along the crystallographic *c*-axis. A P module is depicted by the darker shading. A C module is also labelled in the figure.

of edge shared A and A′ octahedra. Crystals within this family differ from each other largely by the periodicity of the tetrahedra within the chains (tetrahedral repeat) [4]. Crystals with two tetrahedra in the repeat sequence, such as $MgSiO_3$ enstatite, $Ca_{0.5}Mg_{0.5}SiO_3$ diopside, as well as a dense modification of $MnSiO_3$, are called pyroxenes, whereas those with more than two tetrahedra in the repeat sequence, such as $CaSiO_3$ wollastonite with 3, $MnSiO_3$ rhodonite with 5 and $MnSiO_3$ pyroxmangite with 7 tetrahedra in the repeat sequence, are called pyroxenoids. Chain structures within this family have been shown to consist of pyroxene (P) and pyroxenoid $CaSiO_3$ (C) modules (figure 1) [5]. These modules are slices of pyroxene and $CaSiO_3$ (C) cut perpendicular to their respective chain directions. The pyroxene (P) and $CaSiO_3$ (C) modules have segment lengths of two and three corner connected tetrahedral units, respectively. The modules are stacked next to each other in the appropriate sequence perpendicular to the direction of the tetrahedral chains. Pyroxenes and $CaSiO_3$ pyroxenoid consist of an infinite sequence of their respective modules, namely PPP... for pyroxenes and CCC... for $CaSiO_3$ pyroxenoid. $MnSiO_3$ rhodonite consists of an infinite sequence of CP units (CPCPCP...) and the $MnSiO_3$ pyroxmangite modification consists of an infinite sequence of CPP units (CPPCPPCPP...). The repeat unit reflects the periodicity of the tetrahedra in the chain (e.g. CP is $3 + 2 = 5$, which is the tetrahedral repeat in the $MnSiO_3$ rhodonite chain). Transitions between pyroxenoids and pyroxenes are reconstructive, and high temperatures are required to convert pyroxenoids to pyroxenes upon compression [6, 7].

We focus here on the comparative crystal chemical behaviour of these solids at high pressure. In particular we demonstrate a relationship between the medium range order structure (building block sequence) of chain silicates and their transition to either amorphous or dense crystalline solids upon compression. We do this by comparing the results from our compressional study of the pyroxenoid $MnSiO_3$ rhodonite to our principal findings from our high pressure measurements on the pyroxenoids $CaSiO_3$ wollastonite, $MnSiO_3$ pyroxmangite, and the pyroxenes $MgSiO_3$ enstatite, $Ca_{0.5}Mg_{0.5}SiO_3$ diopside, and $MnSiO_3$ (converted from the pyroxenoid at 10 GPa and 1500 K) [8, 9]. We use Raman spectroscopy for monitoring the structural changes in our samples because this technique is sensitive to the structure of both crystalline and non-crystalline solids as well as to changes in coordination of the cations [10].

2. Experimental techniques

Single crystals of $MnSiO_3$ (triclinic, space group $P\bar{1}$, $Z = 10$; Broken Hill, New South Wales, Australia; mineral name: rhodonite), $MnSiO_3$ (triclinic, space group $P\bar{1}$, $Z = 14$; Minas Gerais, Brazil; mineral name: pyroxmangite), $MgSiO_3$ (orthorhombic, space group $Pbca$, $Z = 8$; Smithsonian No. 137311; mineral name: enstatite), $CaSiO_3$ (triclinic, space group $P\bar{1}$, $Z = 6$; Karibib, Namibia; mineral name: wollastonite) and $Ca_{0.5}Mg_{0.5}SiO_3$ (monoclinic, space group $C2/c$, $Z = 4$; De Kalb, New York; mineral name: diopside) [11] were used for all experiments. Pressure was applied with a diamond anvil cell. The crystals with dimensions 10 μm × 50 μm × 20 μm were placed in the centre of tungsten or stainless steel gaskets in an argon pressure medium. The sample chamber dimensions were between 130 and 150 μm in diameter and 60 μm in thickness. The Raman spectra were excited with the 457.9 nm line of an argon ion laser with powers ranging from 5 to 30 mW. The Raman spectra were analysed with a Spex 1402 double monochromator with an LN-cooled CCD (charged coupled device detector). The defocused beam of a 120 W continuous wave CO_2 laser [12] was used for heating the $MnSiO_3$ samples at high pressure in order to convert the $MnSiO_3$ pyroxenoid into its pyroxene analogue [6] and for converting $MgSiO_3$ pyroxene into ilmenite [12]. Heating durations were about 20 min at temperatures of about 1500 K. Pressure was measured using micron sized ruby chips placed next to the samples.

3. Results

3.1. $MnSiO_3$ rhodonite

The high pressure Raman spectra of crystalline $MnSiO_3$ rhodonite are shown in figure 2, including the release spectrum at the top of the figure. The ambient pressure spectra of chain structures spans the region from 200 to 1200 cm^{-1}. The vibrational modes can be classified into three regimes. The regime below 600 cm^{-1} consists of modes associated with countercation (Mn–O, Ca–O, Mg–O) stretches, internal O–Si–O bending, as well as longer wavelength lattice modes. The peaks in the midfrequency region between 600 and 800 cm^{-1} are due to Si–O–Si intertetrahedral stretching and bridging modes, whereas the bands at higher wavenumbers are due to Si–O stretching modes of the non-bridging oxygens in the silica tetrahedra [13, 14]. But the most important transition in the context of our study occurs above 33 GPa, where all Raman modes vanish, indicating formation of a disordered or amorphous state (figure 2). The spectrum was featureless in all regions of the sample examined. Measurements were taken during decompression but the spectrum remains featureless until the sample is recovered outside the diamond cell. The release spectrum was taken using a 5 mW defocused beam to ensure that the sample would not be heated. This spectrum, shown at the top of figure 2, is characteristic of amorphous solids, and is similar to that of melt-quenched glasses in this family [15]. This spectrum was observed from all regions of the sample examined.

3.2. $MnSiO_3$ pyroxmangite, $CaSiO_3$ wollastonite, $Ca_{0.5}Mg_{0.5}SiO_3$ diopside, $MgSiO_3$ enstatite, $MnSiO_3$ pyroxene

Representative high pressure Raman spectra of crystalline $MgSiO_3$, $Ca_{0.5}Mg_{0.5}SiO_3$, $MnSiO_3$ pyroxene, $CaSiO_3$, and the two $MnSiO_3$ pyroxenoid modifications are shown in figures 3(a)–(f), respectively, to illustrate the collective trend exhibited by these chain silicates at very high pressures. A high pressure Raman spectrum of the sixfold coordinated (SiO_6) high pressure and temperature ilmenite phase is also presented in figure 4, to compare to the dense crystalline phases produced at ambient temperature and high pressure. The structures undergo several phase transitions between tetrahedrally (SiO_4) coordinated structures at lower pressures, which

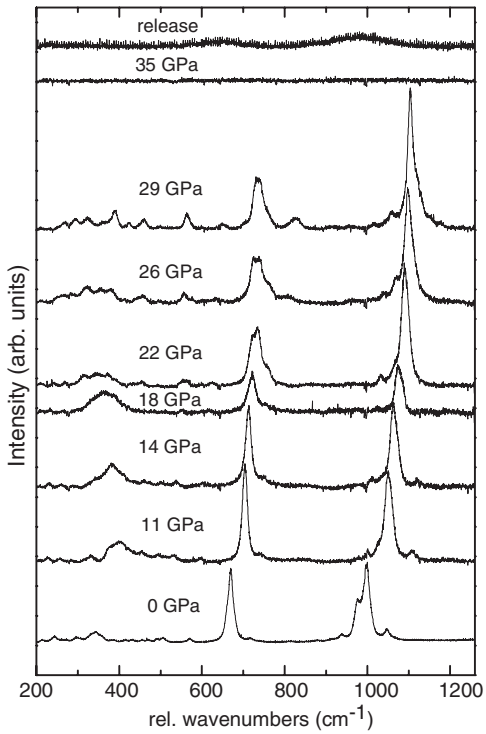

Figure 2. The effect of pressure on the Raman spectrum of $MnSiO_3$ rhodonite showing evidence for a crystal–amorphous transition above 33 GPa. The spectrum of the recovered sample resembles that of melt-quenched chain silicate glasses.

above approximately 35 GPa transform to higher coordinated dense crystalline or amorphous phases [8, 9]. In particular, the pyroxenes transform to higher coordinated crystalline phases (figures 3(a)–(c)), whereas $CaSiO_3$ (figure 3(d)) exhibits both crystalline and amorphous regions at the highest pressures, and the pyroxenoids $MnSiO_3$ rhodonite (figure 3(e)) and pyroxmangite (figure 3(f)) become amorphous above 33 and 35 GPa, respectively. The amorphous regions in $CaSiO_3$ appear in those regions of the sample that experience the largest pressure gradients. The overall mechanism proposed for the transition to the higher coordinated phases is based on the polyhedral tilt model of Stolper and Ahrens [16] for silicate glasses. This mechanism essentially involves a tilting of SiO_4 tetrahedra about their common corners, giving rise to chains of higher coordinated Si–O units. For $MgSiO_3$, $Ca_{0.5}Mg_{0.5}SiO_3$, and $CaSiO_3$, the position and pressure dependency of the intense highest energy non-bridging Si–O stretching modes falls within the regime associated with SiO_6 stretching modes, whereas that for the pyroxene $MnSiO_3$ lies between that for tetrahedral and octahedral stretching vibrations [8, 9, 17, 18]. The higher coordinated crystalline phases revert to their ambient pressure crystalline phases, whereas the featureless Raman regions result in spectra upon release of pressure that resemble those of melt-quenched silicate glasses (topmost spectra in figures 3(d)–(f)).

4. Discussion

Our detailed results on the high pressure behaviour of $MnSiO_3$ rhodonite presented in section 3.1 are consistent with the overview of the compressional behaviour of the chain silicates

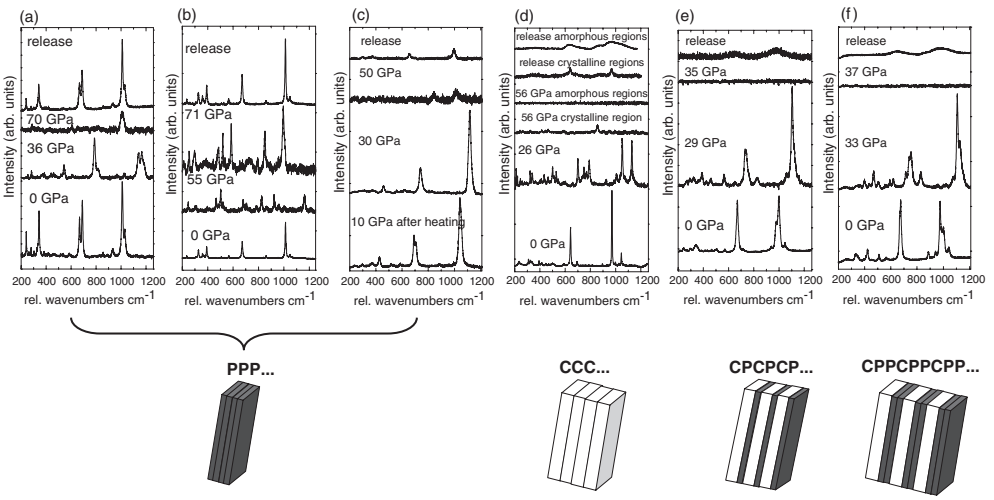

Figure 3. Representative high pressure Raman spectra of the chain silicates $MgSiO_3$ enstatite (a), $Ca_{0.5}Mg_{0.5}SiO_3$ diopside (b), the pyroxene modification of $MnSiO_3$ (c), $CaSiO_3$ wollastonite (d) and the pyroxenoid (rhodonite and pyroxmangite) polymorphs (e), (f) of $MnSiO_3$, and schematic depictions of the ambient pressure phases in terms of their P and C building blocks. The pyroxenes (a)–(c) are made up of an infinite sequence of P modules, $CaSiO_3$ (d) of an infinite sequence of C modules, rhodonite (e) of an infinite sequence of CP modules, and pyroxmangite (f) of an infinite sequence of CPP modules. Depending on their stacking sequence, the crystals transform above 30 GPa to either higher coordinated crystalline or amorphous phases. The pyroxenes $MgSiO_3$ (a) and $Ca_{0.5}Mg_{0.5}SiO_3$ (b) and $MnSiO_3$ (formed from the pyroxenoid polymorph at 10 GPa and 1500 K) undergo reversible transitions to higher coordinated crystalline phases above 40, 55 and 40 GPa, respectively. The pyroxenoid $CaSiO_3$ (d) undergoes a coordination change above 40 GPa, but in the regions where the pressure gradients are larger the vibrational modes vanish (d). Upon release of pressure the spectrum of the ambient pressure phase returns weakly, whereas the featureless regions exhibit a glassy spectrum (d). The pyroxenoid $MnSiO_3$ rhodonite and pyroxmangite polymorph spectra (e), (f) become featureless above 33 and 35 GPa, respectively, and revert to glassy spectra upon release.

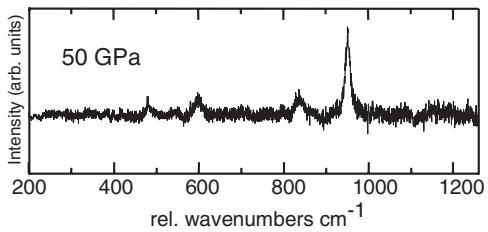

Figure 4. Raman spectrum of $MgSiO_3$ ilmenite synthesized from $MgSiO_3$ enstatite at about 22 GPa and 1500 K. The most intense peak is an octahedral Si–O stretching vibration.

presented in section 3.2. In particular, a consideration of the structural interrelationships between pyroxenoids and pyroxenes and the effect of compositional variation on their crystal structures [19] traces their different response to pressure back to their building block (module) sequence.

Decreasing the countercation size in pyroxenoids (with pressure or composition) favours formation of the pyroxene structure [4]. This is most evident from a study of the crystal structures of several $(Mn_xMg_{1-x})SiO_3$ pyroxenoid compositions [19]. This work shows that the pyroxene (P) modules remain largely undistorted, whereas the pyroxenoid (C) modules become increasingly distorted, as x decreases. These distortions involve kinks in the tetrahedral chains near the C–P boundary, a decrease of non-bonded Si–Si distances below

energetically favourable limits (<3.0 Å) [20], and deformation of octahedral units in the C module [19]. Thus, both C–P interfaces and C modules become unstable with respect to P–P interfaces and P modules as the average countercation size in the slabs decreases. Therefore a pure pyroxene structure becomes favourable as the countercation size decreases (or as the external pressure increases). Previous work shows [7, 21] that the pyroxenoid–pyroxene transition is reconstructive, involving breaking and reforming of Si–O and (Mg, Mn, Ca)–O bonds and redistribution of cations. Incomplete pyroxenoid–pyroxene transformation results in the formation of disordered structures [22, 23]. These disordered structures are documented in a transmission electron microscopy (TEM) study on a natural sample containing both pyroxene and pyroxenoid structures [22].

Pressure generally decreases the size of the countercation polyhedra as compared to the size of the relatively incompressible SiO_4 tetrahedra [24]. Thus, ambient temperature compression of the rhodonite (CPCP...) and pyroxmangite (CPPCPP...) modifications of $MnSiO_3$ pyroxenoid result in distortions in the pyroxenoid structure similar to those described above when smaller magnesium ions replace manganese ions in the structure [19]. These distortions may cause transition to a chain structure of lower symmetry or to a disordered mixture of several chain structures, as observed above for a natural sample using TEM measurements [22]. Above 33 GPa at ambient temperature, transition to new crystalline phases is kinetically impeded for the $MnSiO_3$ pyroxenoids, resulting instead in amorphous phases as shown by our Raman measurements on rhodonite (CPCP...) and pyroxmangite (CPPCPP...) (figures 3(e), (f)). We propose that the absence of pyroxenoid (C) modules and C–P linkages in the pure (PPP...) stacking sequence of the pyroxenes $MnSiO_3$, $MgSiO_3$ and $Ca_{0.5}Mg_{0.5}SiO_3$ allows these structures to accommodate higher pressures without becoming amorphous and instead transforming to denser crystalline structures.

The reason for the presence of both amorphous and octahedrally coordinated crystalline regions above 40 GPa in $CaSiO_3$ may be traced back to its building block sequencing. As discussed above, both C modules and C–P interfaces contribute to the disordering of $MnSiO_3$ pyroxenoid upon compression. $CaSiO_3$ (CCC...), unlike $MnSiO_3$ (CPP...) pyroxenoid, does not contain C–P linkages, which may allow formation of the denser crystalline phase above 40 GPa. This intermediate behaviour is likely promoted first by the existing small pressure gradients at these high pressures and subsequently by the internal stresses caused by the local transition to the denser crystalline phase.

5. Conclusions

The compressional study on rhodonite consolidates the effectiveness of medium range order scale structural criteria (building block sequencing) in predicting pressure-induced phase transformations in an extended family of chain structures. That is, upon compression, chain silicates made of P modules undergo transitions to octahedrally coordinated (SiO_6) crystalline phases; those made of P and C modules become amorphous; those comprised of C modules develop both crystalline and amorphous regions, with the amorphization process being triggered by kinetically impeded C module and C–P interface to P module transitions.

Thus medium range order attributes such as the modular length scale should be considered together with the short and long range structure as well as other attributes including defects, internal strains caused by local volume decreases (phase transitions) as well as external stresses (pressure gradients) in explaining trends in the phase transitions of crystal families.

Acknowledgment

We thank Brian Jackson of the Royal Museum of Scotland for his assistance, useful discussions and donation of the rhodonite crystals.

References

[1] Gaskell P H *et al* 1991 *Nature* **350** 675
[2] Angel R J, Chopelas A and Ross N L 1992 *Nature* **358** 322
[3] Finger L W and Hazen R M 1991 *Acta Crystallogr.* B **47** 561
[4] Liebau F 1985 *Chemistry of Silicates* (Berlin: Springer)
[5] Angel R J and Burnham C W 1991 *Am. Mineral.* **76** 900
[6] Akimoto S and Syono Y 1972 *Am. Mineral.* **57** 76
[7] Angel R J, Price G D and Putnis A 1984 *Phys. Chem. Minerals* **10** 236
[8] Serghiou G, Chopelas A and Boehler R 2000 *J. Phys.: Condens. Matter* **12** 8939
[9] Serghiou G, Boehler R and Chopelas A 2000 *J. Phys.: Condens. Matter* **12** 236
[10] Wolf G H, Durben D J and McMillan P F 1990 *J. Chem. Phys.* **93** 2280
[11] Deer W A, Howie R A and Zussman J 1967 *Rock-Forming Minerals* (London: Longmans)
[12] Boehler R and Chopelas A 1992 *High-Pressure Research: Application to Earth and Planetary Sciences* ed Y Syono and M H Manghnani (Tokyo: Terra Scientific)
[13] Hugh-Jones D, Chopelas A and Angel R 1997 *Phys. Chem. Minerals* **24** 301
[14] Handke M 1986 *Appl. Spectrosc.* **40** 871
[15] Tsunawaki Y *et al* 1981 *J. Non-Cryst. Solids* **44** 369
[16] Stolper E M and Ahrens T 1991 *Geophys. Res. Lett.* **14** 1231
[17] Reynard B and Rubie D C 1996 *Am. Miner.* **81** 1092
[18] Serghiou G 2003 *J. Raman Spectrosc.* **34** 587
[19] Pinckney L R and Burnham C W 1988 *Am. Mineral.* **73** 798
[20] Hill R J and Gibbs G V 1979 *Acta Crystallogr.* B **35** 25
[21] Prewitt C T and Peacor D R 1964 *Am. Mineral.* **49** 1527
[22] Veblen D R 1985 *Am. Mineral.* **70** 885
[23] Veblen D R *et al* 1993 *Science* **260** 1465
[24] Hazen R M and Finger L W 1982 *Comparative Crystal Chemistry* (New York: Wiley)